Chapter 23
Modeling and Performance Analysis of GPS/GLONASS/BDS Precise Point Positioning

Pan Li and Xiaohong Zhang

Abstract The main challenge of dual-frequency precise point positioning (PPP) is that it requires about 30 min to obtain a centimeter level accuracy. Currently, PPP is generally conducted with GPS only using the ionosphere-free combination. Along with the competition of the first phase of the Beidou Navigation Satellite System (BDS) which comprising 5 satellites in Geostationary Orbit (GEO), 5 in Inclined Geosynchronous Orbit (IGSO) and 4 in Medium Earth Orbit (MEO) by the end of 2012, the regional navigation capabilities has been formed and the visibility and availability have been significantly improved for users in the Asia-Pacific regional area. Attention has been paid to improve the performance of PPP by combining BDS and other navigation satellite system (GPS/GLONASS). This study introduces a single-differenced (SD) between-satellite PPP model which can process any single-system or multi-system GNSS (GPS/GLONASS/BDS) raw dual-frequency carrier phase measurements. In this model, the GPS satellite with the highest elevation is selected as the reference satellite to form the SD between-satellite measurements. Thus the GPS receiver clock offset is canceled and only a system time offset between GPS and other GNSS system is estimated for the observations of GLONASS or BDS. In the proposed model, noisy pseudorange measurements are ignored thus modeling the pseudorange stochastic model is not required. The stochastic model for SD measurements and states can be easily realized by mapping that for undifferenced measurements and states. Also the correlation of the SD measurements is considered. Using a 7-day data set from 10 multiple system GNSS stations, we have investigated the performance of single-system PPP, GPS/GLONASS PPP and GPS/GLONASS/BDS PPP, including convergence speed and positioning accuracy. The contribution of BDS observation to the performance of multi-GNSS PPP is analyzed and assessed with special

P. Li (✉) · X. Zhang
School of Geodesy and Geomatics, Wuhan, China
e-mail: lipan.whu@gmail.com

X. Zhang
e-mail: xhzhang@sgg.whu.edu.cn

concern. Numerous experimental results indicate that after adding BDS observations, the convergence time can be reduced by 10–12 % for GPS PPP, and reduced by about 5–7 % for GPS/GLONASS PPP further. Besides, BDS observations can contribute to improving the accuracy of kinematic PPP with 3 h observations. After adding BDS observations, the RMS in kinematic mode is improved by 14.3, 7.1 and 7.5 % for GPS PPP while 11.1, 16.7 and 6.5 % for GPS/GLONASS PPP, in the east, north and up directions, respectively. For GPS/GLONASS/BDS PPP, an accuracy of 1–2 cm in horizontal and 2–3 cm in vertical directions can be achieved in kinematic mode while an accuracy of less than 1 cm in horizontal and 1–2 cm in vertical directions can be achieved in static mode.

23.1 Introduction

Precise Point Positioning (PPP) is one of the representative techniques for high accuracy GNSS-based positioning [1, 2] (the other is Network-based Real-Time Kinematic). Based on pseudorange and carrier phase observations from a stand-alone GNSS receiver and the IGS precise orbit and clock products, PPP positioning accuracy can reach cm- to dm-levels for static or kinematic applications on a global scale. PPP has been demonstrated to be a powerful and efficient technology for scientific and civilian applications, such as near real-time GPS meteorology [3, 4] and crustal deformation monitoring [5, 6]. Although PPP has advantages such as high computational efficiency, not requiring dedicated reference stations, it requires a long convergence time to achieve a desired accuracy. Besides, compared with network double difference solution, PPP suffers from a relative poor accuracy for observations covering a short time interval, such as 3 h [7]. These problems have impeded its further application in many areas and are more significant in the conventional GPS-PPP solution.

Along with the competition of the first phase of the Beidou Navigation Satellite System (BDS) which comprising 5 satellites in Geostationary Orbit (GEO), 5 in Inclined Geosynchronous Orbit (IGSO) and 4 in Medium Earth Orbit (MEO) by the end of 2012, the regional navigation capabilities has been formed and the visibility and availability have been significantly improved for users in the Asia-Pacific regional area. Attention has been paid to improve the performance of PPP with BDS or combining BDS and GPS. Based on simulated data, Yang et al. [8] pointed out the contribution of BDS to user's PNT by analysis of visible satellites and dilution of precision (DOP) values. Shi et al. [9] determined the precise orbit of BDS satellites, with the radial accuracy better than 10 cm; using observations come from a regional reference network named 'Beidou Experimental Tracking Stations' (BETS). Based on achieved orbit and clock products, Shi et al. [9]

showed that static PPP and kinematic RTK can also achieve centimeter level and 5–10 cm respectively. Also with continuous measurement data from BETS, Liu et al. [10] analyzed the impact of different ambiguity resolution strategy on precision orbit determination of BDS and then compared the positioning results of BDS network solution and BDS PPP. The results show that BDS static PPP solution can achieve horizontal accuracy better than 1.4 cm and vertical accuracy better than 3 cm, which is a little worse than BDS network solution, but basically at the same level. Moreover, Li et al. [11] presented an initial performance assessment of dual-frequency un-differenced PPP for GPS, BDS and combined GPS/BDS, using three days datasets of two stations. Their results show that the combined GPS/BDS PPP can shorten the convergence time, but not necessarily improve positioning results by much if the satellites of the single GNSS system already have a good receiver-satellite geometry.

These studies preliminary demonstrated that cm-level positioning accuracy can be achieved using BDS observation covering 24 h. Nowadays, with the recovery of the GLONASS system, many researchers have also studied combined PPP with GPS and GLONASS observations. Their results indicated that the convergence speed can be accelerated by combined PPP [12, 13]. As mentioned above, all these studies are based on dual-system GNSS observations (GPS/GLONASS or GPS/BDS). However, three-system combined PPP with GPS/GLONASS/BDS has not been discussed in the literature until now. Whether three-system combined PPP can shorten the convergence time and improve the positioning accuracy of PPP is an important problem worthy of study and discussion.

This study introduces a single-differenced (SD) between-satellite PPP model which can process any single-system or multi-system GNSS (GPS/GLONASS/BDS) raw dual-frequency carrier phase measurements. In this model, the GPS satellite with the highest elevation is selected as the reference satellite to form the SD between-satellite measurements. Thus the GPS receiver clock offset is canceled and only a system time offset between GPS and other GNSS system is estimated for the observations of GLONASS or BDS. In the proposed model, noisy pseudorange measurements are ignored thus modeling the pseudorange stochastic model is not required. The stochastic model for SD measurements and states can be easily realized by mapping that for undifferenced measurements and states. Based on the post-processing BDS orbit and clock products from Wuhan University GNSS Center (WHU) and GPS/GLONASS products from ESA, and the multi-GNSS observations from MGEX project of IGS and CUTIN university, this contribution aims at investigating the effect of add BDS observations on the positioning performance of GNSS PPP. Also in which, the positioning results of single-system PPP, GPS/GLONASS, GPS/GLONASS/BDS multi-GNSS PPP are compared. In the following sections, the single-differenced-between-satellite PPP algorithm for dual-frequency single and multi-GNSS systems is presented. Then experimental design and data processing strategy are described in Sect. 23.3. In Sect. 23.4, numerical results are presented and analyzed.

23.2 Method

For a satellite s observed by receiver r, the pseudorange and carrier phase observations can be expressed as:

$$P_{r,j}^{s,G} = \rho_r^s + c\left(dt_r^G - dt^{s,G}\right) + T^{s,G} + I_{r,j}^{s,G} + B_{r,j}^G - B_j^{s,G} + e_{r,j}^{s,G} \quad (23.1)$$

$$L_{r,j}^{s,G} = \rho_r^s + c\left(dt_r^G - dt^{s,G}\right) + T^{s,G} - I_{r,j}^{s,G} + \lambda_j^G\left(N_{r,j}^{s,G} + b_{r,j}^G - b_j^{s,G}\right) + \varepsilon_{r,j}^{s,G} \quad (23.2)$$

where G refers to a satellite system (GPS/GLONASS/BDS, etc.); the subscript $j(=1, 2)$ refers to a given frequency; ρ is the geometric distance; c is the speed of light; dt_r and dt^s are the clock errors of receiver and satellite, respectively; T is the slant troposphere delay; $I_{r,j}^s$ is the slant ionospheric delay at the j frequency; N is the integer ambiguity; $b_{r,j}$ and b_j^s are the receiver-dependent and satellite-dependent uncalibrated phase delays (UPD) at the j frequency, respectively; λ_j is the wavelength of the frequency j; $B_{r,j}$ is the signal delay from receiver antenna to the signal correlator in the receiver; B_j^s is signal delay from satellite signal generation to signal transmission from satellite antenna; e is the pseudorange measurement noise; ε is measurement noise of carrier phase.

23.2.1 A Simple Review on Undifferenced PPP Model

Ionosphere-free combination observables are normally used in PPP to eliminate the first-order ionospheric delays in the pseudorange and carrier phase measurements. The undifferenced ionosphere-free GPS PPP model has been well presented and discussed in detail by many authors such as Kouba and Héroux [1], Zumberge et al. [2]. Furthermore, one can refer to Cai and Gao [12], Li et al. [11] for a clear study on the undifferenced ionosphere-free combined GPS/GLONASS, GPS/BDS PPP model, including both functional and stochastic components.

In undifferenced PPP, the pseudorange should be assigned with an appropriate weight to separate the receiver clocks and the ambiguities, especially for GLONASS. As reported by Cai and Gao [12], the GLONASS code observation residuals are about twice as large as those of GPS, caused by GLONASS satellite-dependent code hardware delay and errors in the GLONASS precise products. Hence, they empirically assign about half the weights of GPS code observations to GLONASS code observations to weaken the effect of larger GLONASS code observation residuals on the positioning results. How to suitably model the code observation to mitigate the impact of multipath, code hardware delay is still a research question to high-precision PPP.

Moreover for combined PPP model with multi-GNSS observations, instead of estimating a receiver clock parameter for each satellite system observation, it is preferable to introduce a system time difference parameter as it can reflect the

difference between different system times. Therefore a receiver clock error for GLONASS and BDS can be described as follows, when they are integrated with GPS:

$$dt_r^{GLO} = dt_r^{GPS} + dt_{r\_sys}(GPS - GLO) \tag{23.3}$$

$$dt_r^{BDS} = dt_r^{GPS} + dt_{r\_sys}(GPS - BDS) \tag{23.4}$$

where $dt_{r\_sys}(GPS - GLO)$ is the GPS-GLONASS system time difference while $dt_{r\_sys}(GPS - BDS)$ denotes the GPS-BDS system time difference.

23.2.2 Functional Model of Single-Difference Between-Satellite PPP

In fact, for most applications except for time transfer [14], the receiver clock offsets are often not of concern and can be ignored. Therefore, we apply the single-difference between-satellite on the undifferenced ionosphere-free carrier phases to eliminate the GPS receiver clocks errors and the receiver-dependent uncalibrated phase delays (UPD) [15]. In this SD model, no epoch-wise receiver clock parameter need to be estimated in single-system PPP because the receiver clock offset is eliminated. While in multi-system PPP the system time offset between GPS and GLONASS is estimated for the GLONASS observations and that between GPS and BDS is estimated for the BDS observations. In this case we do not need pseudorange measurements to separate the receiver clocks and the ambiguities so that we do not need to rigorously model the pseudorange measurements.

Specifically, our PPP algorithm implementation is based on a Kalman-filter. The filter processes SD ionosphere-free linear combinations of carrier phase measurements. The satellite with healthy observations and the highest elevation is selected as the reference for single-system PPP. However, for multi-GNSS PPP involving GPS, the GPS satellite with healthy observations and the highest elevation is selected as the reference. Assuming m satellites were simultaneously tracked by receiver r, then the linearized equations for the undifferenced carrier phase observation of all satellites can be formed as follows:

$$\underset{m\times1}{y} = \underset{m\times(m+6)}{A} \cdot \underset{(m+6)\times1}{x} + \underset{m\times1}{\varepsilon_y}, \quad \varepsilon_y \sim N(0, Q_{yy}) \tag{23.5}$$

$$x = \left[X, Y, Z, ZWD, dt_{r\_sys}(GPS - GLO), dt_{r\_sys}(GPS - BDS), N_{if}^s\right]^T \tag{23.6}$$

SD measurements can be easily formed by mapping that of undifferenced measurements using the transformation matrix. With this method, the correlation of the SD measurements is also considered. The unknown vector in the PPP includes three position coordinate, a wet zenith tropospheric delay (ZWD), two system time

offset $dt_{r\_sys}(GPS - GLO)$ and $dt_{r\_sys}(GPS - BDS)$ (fixed to zero if no observation from corresponding satellite system) and the undifferenced float ambiguities N_{if}^s, where $s = 1 \ldots m$. The quantity Q_{yy} takes the form of a diagonal matrix with its diagonal elements $Q_{ii} = \sigma_0^2 / \sin^2(E_r^s)$, E_r^s is the elevation angle of each satellite and σ_0 is the standard deviation of the GNSS observation at zenith.

23.2.3 Stochastic Model of Single-Difference Between-Satellite PPP

The Extended Kalman Filter (EKF) is utilized in the parameter estimation, and the corresponding dynamic model can be denoted as:

$$x(i + 1) = \Phi_{i+1,i} \cdot x(i) + \omega(i), \quad \omega \sim N(0, Q_{\omega\omega}) \tag{23.7}$$

$\Phi_{i+1,i}$ is the corresponding transition matrix, ω is the normally-distributed process noise with zero-mean and variance-covariance (VC) matrix $Q_{\omega\omega}$. The matrix $Q_{\omega\omega}$ can be denoted as:

$$Q_{\omega\omega} = diag\left\{ q_p \cdot \Delta t, q_{zwd} \cdot \Delta t, q_{t(GPS/GLO)} \cdot \Delta t, q_{t(GPS/BDS)} \cdot \Delta t, \underset{m \times m}{0} \right\} \tag{8}$$

where Δt is the time interval between adjacent epochs. For the Kalman filter, the spectral density values for the ZWD and the system time difference parameter are empirically set to $q_{zwd} = 10^{-8}$ m²/s and $q_{t(GPS/GLO)} = q_{t(GPS/BDS)} = 10^{-6}$ m²/s, respectively. The ambiguity parameters and static position coordinates are considered as constants. But in kinematic mode, the kinematic position coordinates are modeled as white noise and the diagonal element of q_p is 10^4 m²/s. The initial standard deviation values for phase observations of three GNSS systems are all set to 0.003 m. During the filtering, the state vector is predicted from the previous epoch to the current epoch using a system model. The state vector and the associated covariance matrix are then resolved with the observations in the measurement update process.

23.3 Data Processing and Experimental Strategy

GNSS measurements recorded in 30-s intervals from about 10 stations observed during DOY 264 to 270 in 2013 are used in this study (Table 23.1). Precise final GPS/GLONASS satellite orbit and clock corrections are provided by the European Space Agency (ESA) while the final BDS orbits and clock products are provided

Table 23.1 The information of stations

| Site	Lat (°)	Lon (°)	Receive type	Antenna type	Agency
CUAA	−32.0	115.9	JAVAD TRE_G3T DELTA	TRM59800.00 SCIS	Curtin Univ
CUBB	−32.0	115.9	JAVAD TRE_G3T DELTA	JAV_GRANT-G3T NONE	Curtin Univ
CUT1	−32.0	115.9	SEPT POLARX4	TRM59800.00 SCIS	Curtin Univ
CUT2	−32.0	115.9	TRIMBLE NETR9	TRM59800.00 SCIS	Curtin Univ
CUT3	−32.0	115.9	JAVAD TRE_G3T DELTA	TRM59800.00 SCIS	Curtin Univ
GMSD	30.6	131.0	TRIMBLE NETR9	TRM59800.00 SCIS	IGS
JFNG	30.5	114.5	TRIMBLE NETR9	TRM59800.00 NONE	IGS
KZN2	55.8	49.1	TRIMBLE NETR9	TRM59800.00 SCIS	IGS
NNOR	−31.0	116.2	SEPT POLARX4	SEPCHOKE_MC NONE	IGS
REUN	−21.2	55.6	TRIMBLE NETR9	TRM55971.00 NONE	IGS

by Wuhan University GNSS Research Center. We also apply the absolute antenna phase centers model [16]. The 'antex' file generated and released by the International GNSS Service (IGS) which includes Phase Center Offset (PCO) and Phase Center Variation (PCV) corrections information for both satellites and receivers are used for precise data processing. It should be mentioned that only a preliminary PCO of BDS satellites is available for BDS from IGS, therefore, PCO and PCV corrections cannot be corrected for BDS observations accurately. The elevation cut-off angle is set to 7°.

For each station, the 24 h dataset is divided into 8 sessions, so each session is 3 h. This length of data should be long enough to ensure the convergence of the position solutions in most cases. The processing results of the first 90 min of observations are mainly used for analyzing the convergence time, while the results of the second 90 min of observations are mainly used for analyzing the positioning accuracy. In this study, "convergence" means "obtaining a 3D positioning error less than 1 dm". The positioning error is just the difference of the position solution and the true coordinate benchmarks from IGS weekly solution. We also check the errors of 20 epochs after. Only when the errors of all 20 epochs are within the limit, we consider the position has converged in this epoch [13].

23.4 Experimental Results and Analysis

In total there are about 560 positioning tests used in the experiment. The positioning performance of single- and multi-system PPP is analyzed based on different processing models, namely GPS-only, GLONASS-only, BDS-only, combined GPS/GLONASS, combined GPS/BDS and combined GPS/GLONASS/BDS PPP.

Fig. 23.1 Convergence time
of kinematic PPP for the
observations of the 3rd
session from station REUN
on DOY 264, 2013
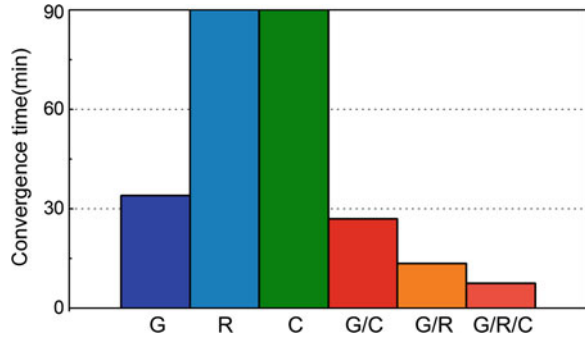
23.4.1 The Convergence Speed Results

The forward-Kalman-filter PPP is applied to all 3-h-long observations in both the
static and kinematic mode. The convergence time of each solution is recorded.

First we take the kinematic PPP results of the 3rd session from REUN station
on DOY 264, 2013 as a typical example to compare the convergence time of six
processing models. Details are given in Fig. 23.1. We can find that over 90 min are
required to achieve the convergence for GLONASS-PPP and BDS-PPP, while only
34.0 min are needed for GPS-PPP. Compared with GPS-PPP, the convergence
time is reduced by 7 min in GPS/BDS PPP while compared with GPS/GLONASS-
PPP; the convergence time is reduced by 6 min in GPS/GLONASS/BDS PPP.
Hence a faster convergence speed is achieved by adding BDS observation.

Figure 23.2 shows the average convergence time of kinematic PPP on each day
over all test stations. For each PPP model, the average convergence time shows a
good agreement over days. There are no significant daily variations in the average
convergence time. The average convergence time of static PPP also had the same
rule. Similar phenomenon can be also found in static PPP.

Statistical results of the convergence time for all observations are plotted in
Fig. 23.3 for static and kinematic PPP. As can be seen, in static mode, the average
convergence time is 25.7 min for GPS-PPP, which is obviously shorter than that of
GLONASS-PPP and BDS-PPP. For GPS-PPP, the convergence time can be further
reduced by 10.5 % by adding BDS observation and by 38.9 % by adding
GLONASS observation. A shortest convergence time of 15.0 min is achieved by
three-system PPP. Compared with that of GPS/GLONASS PPP, the convergence
time is further improved by 4.5 % after adding BDS observations. Owing to a
relatively weaker model, the average convergence time of kinematic PPP is sig-
nificantly longer than that of static PPP, for single- and multi- system solutions.
The statistical results of kinematic PPP are as follows: The average convergence
time is 45.1 min for GPS PPP while 39.6 min for GPS/BDS PPP. It is reduced
significantly by 12.2 % after adding BDS observations. The average convergence
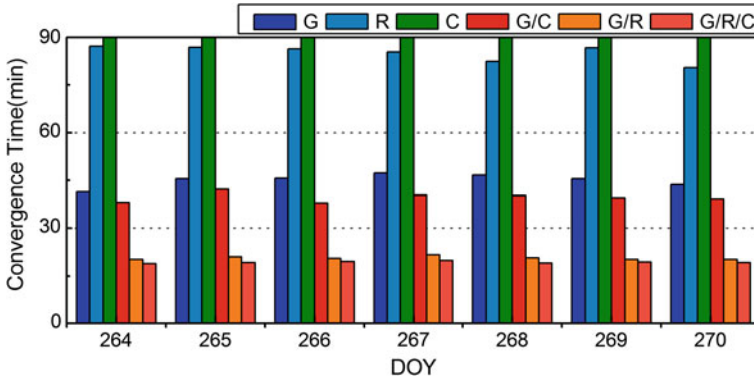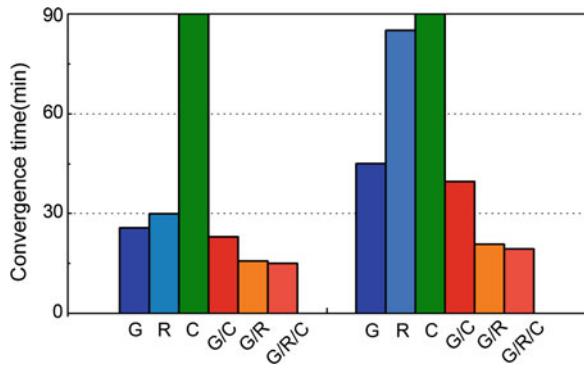time is 20.7 min for GPS/GLONASS PPP while 19.3 min for GPS/GLONASS/

Fig. 23.2 Average convergence time of kinematic PPP per day

Fig. 23.3 Average convergence time of static (*left*) and kinematic (*right*) PPP

BDS PPP. It is reduced further by 6.8 % with BDS observations combined. As shown, the overall convergence time is reduced more significantly compared to static PPP. This is because adding BDS observations leads to enhancement of strength of geometry and redundancy in kinematic PPP.

As we know, PPP solutions are sensitive to satellite orbit and clock products and the error correction model. Currently, the Beidou orbit and clock products from WHU have a lower accuracy than GPS/GLONASS products from ESA. Moreover, PCO and PCV, one of the major error sources, cannot be corrected accurately for BDS observations. Therefore, the convergence time of BDS-PPP is longer than GPS-PPP and GLONASS-PPP and compared with GLONASS, BDS has a smaller contribution to rapid convergence to combined PPP in current situation.

Table 23.2 Average RMS of all tests in east, north and up directions for static PPP (cm)

	G	R	C	G/ C	G/ R	G/R/ C
E	1.5	3.0	9.8	1.5	0.9	0.9
N	0.6	1.1	5.5	0.6	0.5	0.5
U	1.6	2.5	17.0	1.6	1.5	1.4

23.4.2 The Positioning Accuracy Results

In this part, the positioning accuracy of single- and multi-system PPP solutions is compared. We have calculated the root mean square (RMS) values of the positioning biases over all sessions. For static PPP, as shown in Table 23.2, the average RMS of conventional GPS-PPP solution is only 1.5, 0.6 and 1.6 centimeters in the east, north and up directions, respectively. The highest positioning accuracy is achieved by three-system PPP. We find that it has nearly no impact on the positioning accuracy whether adding BDS observation or not. This is because that the model strength of static PPP is strong enough so that the effect of the low-precision BDS observation can be negligible. A higher positioning accuracy is expected if exact PCO and PCV information is provided for BDS and precise clock offset and orbit of BDS satellites are routinely provided with a precision of several centimeters.

For kinematic PPP, we first take the 3-h-long observation of the 1st session from CUT2 station on DOY 264, 2013 as a representative example to analyze the positioning performance of different PPP models. The epoch-wise coordinate biases in three directions are plotted in Fig. 23.4. The bias in up direction gets larger from 300th to 360th epoch for GLONASS PPP. Only a dm-level positioning accuracy can be obtained by BDS-PPP. The positioning bias of GPS-PPP is relatively smaller and stable compared with GLONASS-PPP and BDS-PPP. Combining multi-GNSS observations, a more stable and accuracy positioning results can be obtained. Furthermore, the epoch-wise 3D coordinate biases are given in Fig. 23.5. It clearly shows that, BDS observation can contribute to improving positioning accuracy, no matter combined with GPS or GPS/GLONASS. The best positioning results with a precision of 2–3 cm is achieved by GPS/ GLONASS/BDS PPP.

We have calculated the average RMS of all sessions; see Table 23.3. Comparing GPS-PPP and GPS/BDS-PPP, we find that the RMS can be improved by 14.3, 7.1 and 7.5 % in east, north and vertical directions after BDS observation is involved in the processing. Besides, Comparing GPS/GLONASS-PPP and GPS/ GLONASS/BDS-PPP, we can find that the RMS can be further improved by 11.1, 16.7 and 6.5 % in three directions after BDS observation is involved in the processing. For each PPP model, the accuracy of the east component is considerably worse than that of the north component because that the integer ambiguity have not be correctly resolved. Generally speaking, the accuracy of the east component is lower than that of north component for a PPP float solution [17, 18].
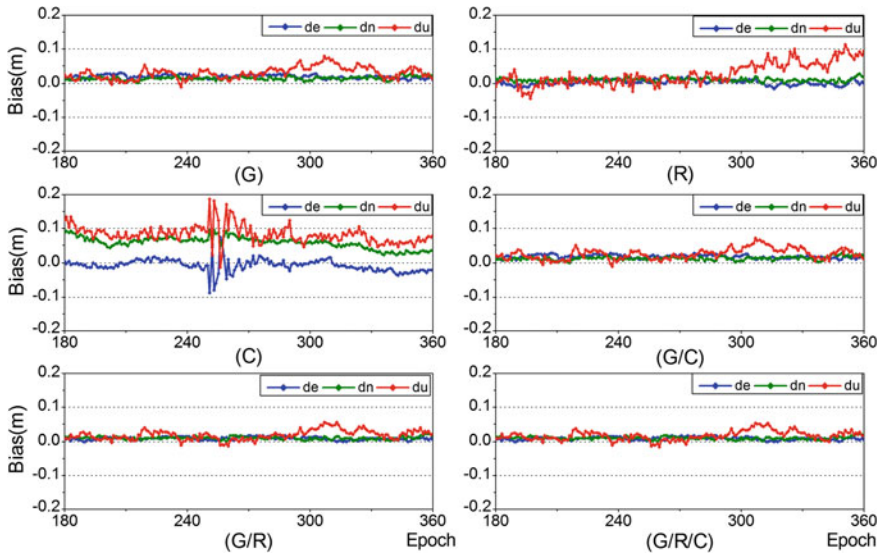
Fig. 23.4 Coordinate biases of kinematic PPP for the observations of the 1st session from station CUT2 on DOY 264, 2013, with different PPP models, in east, north and up directions, respectively

Fig. 23.5 3D coordinate biases of kinematic PPP for the observations of the 1st session from station CUT2 on DOY 264, with different PPP models
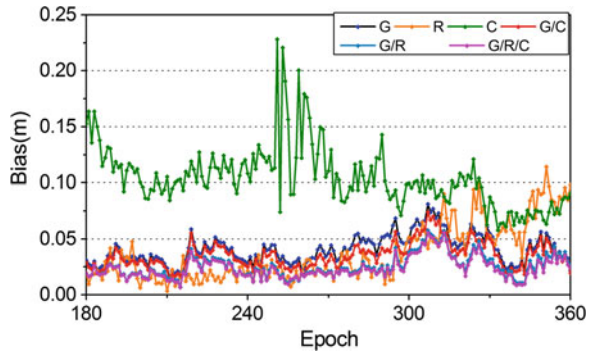

Table 23.3 Average RMS of all tests in east, north and up directions for kinematic PPP (cm)

	G	R	C	G/C	G/R	G/R/C
E	2.8	16.5	26.1	2.4	1.8	1.6
N	1.4	6.7	14.3	1.3	1.2	1.0
U	4.0	21.6	37.1	3.7	3.1	2.9

23.5 Conclusions and Remarks

This study introduces a single-differenced between-satellite precise point positioning model which can process single or multiple system GNSS (GPS/GLONASS/BDS) raw dual-frequency carrier phase measurements. Based on the BDS products from WHU and GPS/GLONASS products from ESA, about 560 3 h-long datasets have been used in the numerical analysis and the positioning results of single- and multi-GNSS PPP are reported. The main conclusions are as followed:

1. Adding BDS observations can contribute to accelerating the convergence speed of PPP. The convergence time can be reduced by 10–12 % for GPS PPP, and reduced by about 5–7 % for GPS/GLONASS PPP further, after adding BDS observation. A shortest convergence time is achieved by three-system PPP.
2. BDS observations can contribute to improving the accuracy of kinematic PPP with 3 h observations. After adding BDS observations, the RMS in kinematic mode is improved by 14.3, 7.1 and 7.5 % for GPS PPP while 11.1, 16.7 and 6.5 % for GPS/GLONASS PPP, in the east, north and up directions, respectively. For GPS/GLONASS/BDS PPP, an accuracy of 1–2 cm in horizontal and 2–3 cm in vertical can be achieved in kinematic mode while an accuracy of less than 1 cm in horizontal and 1–2 cm in vertical can be achieved in static mode.

The performance of multi-GNSS PPP is expected to be further improved with more accuracy of precise products and exact PCO and PCV information provided for BDS in future.

References

1. Kouba J, Héroux H (2001) Precise point positioning using IGS orbit and clock products. GPS Solutions 5(2):12–28
2. Zumberge J, Heflin M, Jefferson D, Watkins M, Webb F (1997) Precise point positioning for the efficient and robust analysis of GPS data from large networks. J Geophys Res 102(B3):5005–5017
3. Gendt G, Dick G, Reigber C, Tomassini M, Liu Y, Ramatschi M (2004) Near real time GPS water vapor monitoring for numerical weather prediction in Germany. J Meteorol Soc Japan. Ser. II 82(1B):361–370
4. Rocken C, Johnson J, Van Hove T, Iwabuchi T (2005) Atmospheric water vapor and geoid measurements in the open ocean with GPS. Geophys Res Lett 32(12):L12813

5. Calais E, Han JY, DeMets C, Nocquet JM et al (2006) Deformation of the North American plate interior from a decade of continuous GPS measurements. J Geophys Res 111:B6402
6. Hammond WC, Thatcher W (2005) Northwest basin and range tectonic deformation observed with the global positioning system, 1999–2003. J Geophys Res Solid Earth 110(B10405B10)
7. Zhang XH, Li P, Guo F (2013) Ambiguity resolution in precise point positioning with hourly data for global single receiver. Adv Space Res 51(1):153–161
8. Yang YX, Li JL, Xu JY, Tang J, Guo HR, He HB (2011) Contribution of the Compass satellite navigation system to global PNT users. Chin Sci Bull 56(26):2813–2819. doi:10.1007/s11434-011-4627-4
9. Shi C, Zhao QL, Li M, Tang WM, Hu ZG, Lou YD, Zhang HP, Niu XJ, Liu JN (2012) Precise orbit determination of Beidou satellites with precise positioning. Sci China Earth Sci 55(7):1079–1086
10. Liu Y, Lou Y, Shi C et al (2013) BeiDou regional navigation system network solution and precision analysis. In: Proceedings of the 4th China satellite navigation conference (CSNC), Wuhan, China, 15–17 May 2013
11. Li W, Teunissen PJG, Zhang B, Verhagen S (2013) Precise point positioning using GPS and Compass observations. In: Proceedings of the 4th China satellite navigation conference (CSNC), Wuhan, China, 15–17 May 2013
12. Cai C, Gao Y (2013) Modeling and assessment of combined GPS/GLONASS precise point positioning. GPS Solutions 17(2):223–236
13. Li P, Zhang XH (2013) Integrating GPS and GLONASS to accelerate convergence and initialization times of precise point positioning. GPS Solutions. doi:10.1007/s10291-013-0345-5
14. Defraigne P, Baire Q (2011) Combining GPS and GLONASS for time and frequency transfer. Adv Sp Res 47(2):265–275
15. Blewitt G (1989) Carrier phase ambiguity resolution for the global positioning system applied to geodetic baselines up to 2000 km. J Geophys Res 94(B8):10187–10203
16. Rebischung P, Griffiths J, Ray J, Schmid R, Collilieux X, Garayt B (2012) IGS08: the IGS realization of ITRF2008. GPS Solutions 16(4):483–494
17. Ge M, Gendt G, Rothacher M, Shi C, Liu J (2008) Resolution of GPS carrier-phase ambiguities in precise point positioning (PPP) with daily observations. J Geodesy 82(7):389–399
18. Zhang XH, Li P (2013) Assessment of correct fixing rate for precise point positioning ambiguity resolution on global scale. J Geodesy 87(6):579–589